ELSEVIER

27 December 2001

PHYSICS LETTERS B

Physics Letters B 523 (2001) 273–279

www.elsevier.com/locate/npe

# N* electroproduction amplitudes in a model with dynamical confinement

P. Alberto [a,b], M. Fiolhais [a,b], B. Golli [c], J. Marques [b]

[a] *Department of Physics, University of Coimbra, P-3004-516 Coimbra, Portugal*
[b] *Centre for Computational Physics, University of Coimbra, P-3004-516 Coimbra, Portugal*
[c] *Faculty of Education, University of Ljubljana, and J. Stefan Institute, Ljubljana, Slovenia*

Received 15 March 2001; received in revised form 15 October 2001; accepted 9 November 2001
Editor: R. Gatto

**Abstract**

The Roper resonance is described in a chiral version of the chromodielectric model as a cluster of three quarks in radial–orbital configuration $(1s)^2(2s)^1$, surrounded by $\pi$- and $\sigma$-meson clouds and by a chromodielectric field which assures quark dynamical confinement. Radial profiles for all fields are determined self-consistently for each baryon. Transverse $A_{1/2}$ and scalar $S_{1/2}$ helicity amplitudes for the nucleon–Roper transition are calculated. The contribution of glueball and $\sigma$-meson vibrations is estimated; although small for N(1440), the $\sigma$ contribution can be large for N(1710). 

*PACS:* 12.39.Fe; 13.40.Gp; 14.20.Gk

The new facilities for intermediate energy nuclear physics, operating with continuous electron beams, make more accessible accurate measurements of electromagnetic properties of both the nucleon and excited states, thus providing more and better information on the structure of baryons, and stimulating theoretical research on the structure of the nucleons and its resonances. The Roper resonance, N(1440), is of particular interest since, due to its relatively low excitation energy, a simple picture in which one quark populates the 2s level does not work here. The constituent quark model (CQM) does not yield sensible results for the electromagnetic properties unless the quark dynamics is treated relativistically [1,2] and, furthermore, approximations beyond the simple Gaussian approximation [3], or inclusion of $q\bar{q}$ pairs [4] are taken into account. These difficulties suggest that additional degrees of freedom, such as explicit excitations of gluefield [5], glueball field [6], or chiral fields [7–9] may be important for formation of the Roper resonance.

In this Letter we use a simple model, the chromodielectric model (CDM), which is particularly suitable to describe the interplay of glueball and meson excitations together with the usual quark radial excitation. In contrast to the nonrelativistic or relativistic versions of the constituent quark model, in the CDM the electromagnetic current operator is derived directly from the Lagrangian, hence no additional assumptions have to be introduced in the calculation of electroexcitation amplitudes. The electromagnetic current contains an explicit contribution from the pion field which has

*E-mail addresses:* pedro@teor.fis.uc.pt (P. Alberto), tmanuel@teor.fis.uc.pt (M. Fiolhais), bojan.golli@ijs.si (B. Golli), jpcmarques@hotmail.com (J. Marques).

0370-2693/01/$ – see front matter 
PII: S0370-2693(01)01348-X

been shown to play an important role in the description of the N–Δ electroproduction [10].

The Roper has been considered in a non-chiral version of the CDM using the RPA techniques to describe coupled vibrations of valence quarks and the background chromodielectric field [6]. The energy of the lowest excitation turned out to be 40% lower than the pure 1s–2s excitations. A similar result was obtained by Guichon [11], using the MIT bag model and considering the Roper as a collective vibration of valence quarks and the bag.

In our approach we describe the nucleon and the Roper as chiral solitons resulting from the non-linear interactions between quarks and a scalar–isoscalar chiral singlet field $\chi$ which, through the peculiar way it couples to the quarks, provides a mechanism for confinement. In addition, the quarks interact with scalar–isoscalar ($\sigma$) and pseudoscalar–isovector ($\vec{\pi}$) mesons similarly as in the linear $\sigma$-model, though in the CDM the chiral fields are weaker and similar to the solution in the CBM for bag radius above 1 fm. The Lagrangian of the model can be written as [12]

$$\mathcal{L} = \mathcal{L}_q + \mathcal{L}_{\sigma,\pi} + \mathcal{L}_{q-\text{meson}} + \mathcal{L}_\chi, \tag{1}$$

where

$$\mathcal{L}_q = \mathrm{i}\bar{\psi}\gamma^\mu\partial_\mu\psi,$$
$$\mathcal{L}_{\sigma,\pi} = \frac{1}{2}\partial_\mu\hat{\sigma}\partial^\mu\hat{\sigma} + \frac{1}{2}\partial_\mu\hat{\vec{\pi}}\cdot\partial^\mu\hat{\vec{\pi}} - \mathcal{U}\big(\hat{\vec{\pi}}^2+\hat{\sigma}^2\big), \tag{2}$$

$\mathcal{U}(\hat{\vec{\pi}}^2+\hat{\sigma}^2)$ being the usual Mexican hat potential, and the quark–meson interaction is given by

$$\mathcal{L}_{q-\text{meson}} = \frac{g}{\chi}\bar{\psi}\big(\hat{\sigma} + \mathrm{i}\vec{\tau}\cdot\hat{\vec{\pi}}\gamma_5\big)\psi. \tag{3}$$

The last term in (1) contains the kinetic and the potential piece for the $\chi$-field:

$$\mathcal{L}_\chi = \frac{1}{2}\partial_\mu\hat{\chi}\partial^\mu\hat{\chi} - \frac{1}{2}M^2\hat{\chi}^2. \tag{4}$$

Other versions of the CDM consider a quartic potential in (4). By taking just the mass term the confinement is imposed in the smoothest way, which seems to be the most appropriate choice for the quark matter sector of the CDM [13].

The parameters of the model have been fixed by requiring that the calculated static properties of the nucleon agree best with the experimental values: we take $g = 0.03$ GeV and $M = 1.4$ GeV [10,13,14]. The pion decay constant and the chiral meson masses are fixed to $f_\pi = 0.093$ GeV and $m_\pi = 0.14$ GeV, while for the mass of the $\sigma$-meson we consider values between $m_\sigma = 0.7$ GeV and $m_\sigma = 1.2$ GeV. We have checked that our results depend very weakly on the variations of these parameters.

The starting point to describe a baryon is the hedgehog coherent state, which we write in the form:

$$\begin{aligned}|Hh\rangle = N\exp\Bigg\{&\sum_{tm}(-1)^m\delta_{t,-m}\\ &\times\int_0^\infty \mathrm{d}k\sqrt{\frac{2\pi\omega_\pi(k)}{3}}\,\xi(k)a^\dagger_{tm}(k)\Bigg\}\\ \times\exp\Bigg\{&\int_0^\infty \mathrm{d}k\sqrt{2\pi\omega_\sigma(k)}\,\eta(k)\tilde{a}^\dagger(k)\Bigg\}\\ \times\exp\Bigg\{&\int_0^\infty \mathrm{d}k\sqrt{2\pi\omega_\chi(k)}\,\zeta(k)b^\dagger(k)\Bigg\}\\ \times&\prod_{i=1,3}c^\dagger_h(i)|0\rangle.\end{aligned} \tag{5}$$

Here $a^\dagger_{tm}(k)$ is the creation operator for a p-wave pion with isospin and angular momentum third components $t$ and $m$, respectively, orbital wave function $\xi(k)$ and frequency $\omega_\pi = \sqrt{k^2+m_\pi^2}$; similarly, $\tilde{a}^\dagger(k)$ and $b^\dagger(k)$ create s-wave $\sigma$ and $\chi$ quanta, with orbital wave functions $\eta(k)$ and $\zeta(k)$, and frequencies $\omega_\sigma$ and $\omega_\chi$, respectively; $N$ is a normalization constant. The amplitudes, $\xi(k)$, $\eta(k)$ and $\zeta(k)$, are Fourier transforms of the corresponding pion, $\sigma$ and $\chi$ radial profiles, which we denote as $\phi(r)$, $\sigma(r)$, and $\chi(r)$, respectively. Finally, the operator $c^\dagger_h(i)$ creates a s-wave valence quark in a spin–isospin hedgehog state:

$$\langle\boldsymbol{r}|c^\dagger_h(i)|0\rangle = q_i(\boldsymbol{r}) = \frac{1}{\sqrt{4\pi}}\begin{pmatrix}u_i(r)\\ \mathrm{i}v_i(r)\boldsymbol{\sigma}\cdot\hat{\boldsymbol{r}}\end{pmatrix}|h\rangle,$$
$$|h\rangle = \frac{1}{\sqrt{2}}\big(|u\downarrow\rangle - |d\uparrow\rangle\big). \tag{6}$$

The index $i$ distinguishes between different radial states. The physical states are obtained by performing the Peierls–Yoccoz projection [15]:

$$|\mathrm{N}_{1/2,M_T}\rangle = \mathcal{N}P^{1/2}_{1/2,-M_T}|Hh\rangle,$$
$$|\mathrm{R}'_{1/2,M_T}\rangle = \mathcal{N}'P^{1/2}_{1/2,-M_T}|Hh^*\rangle. \tag{7}$$

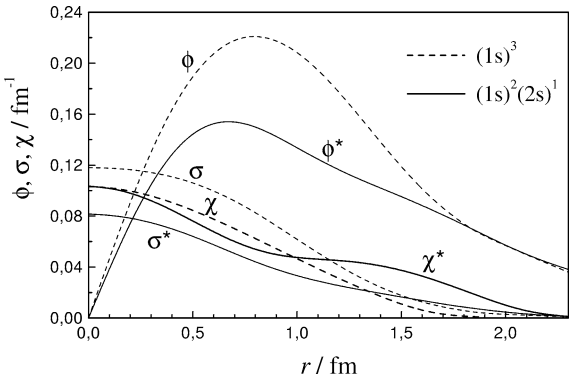


Fig. 1. Self-consistent chromodielectric field and chiral (pion and sigma) fields for quark configurations $(1s)^3$ ($\chi$) and $(1s)^2(2s)^1$ ($\chi^*$). The represented sigma profile is its fluctuation from the vacuum $-f_\pi$. We used the parameter set $g = 0.03$ GeV, $M = 1.4$ GeV and $m_\sigma = 0.85$ GeV.

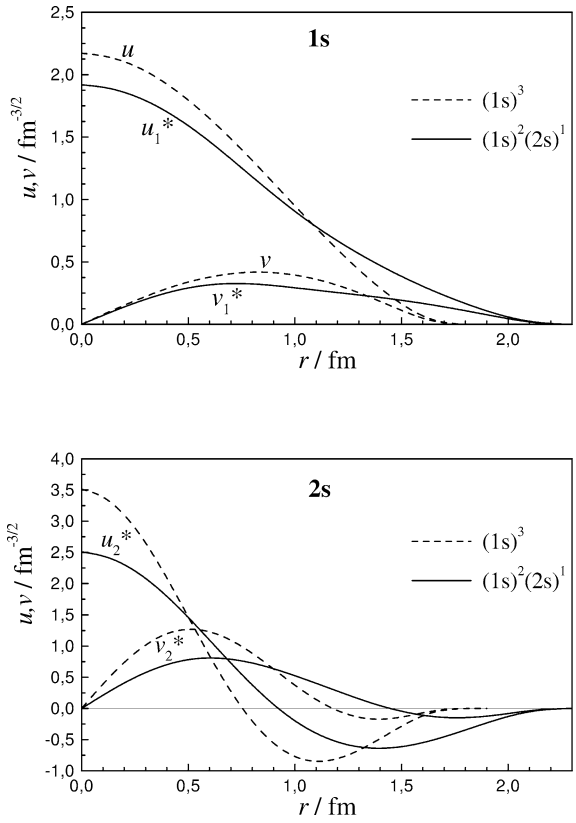


Fig. 2. Quark radial profiles of 1s state and 2s states for $(1s)^3$ and $(1s)^2(2s)^1$ configurations. The dashed curves on the lower panel were computed using frozen ground-state meson fields. The full curves in the lower panel as well as all curves in the upper panel were determined self-consistently. Same parameters as in Fig. 1.

The $\chi$- and the $\sigma$-fields are not affected by projection. The radial profiles $\phi(r)$, $\sigma(r)$ and $\chi(r)$, and the quark profiles are determined self-consistently using variation after projection [12], separately for the nucleon and for the Roper. For the Roper, one has still to distinguish between the radial functions for quarks in 1s state and in 2s state, and we shall use the self-explanatory notation $u_1^*$, $v_1^*$, $u_2^*$, $v_2^*$, $\sigma^*$, $\phi^*$ and $\chi^*$. The states (7) are normalized but not mutually orthogonal. They can be orthogonalized by taking

$$|\mathrm{R}\rangle = \frac{1}{\sqrt{1-c^2}}\big(|\mathrm{R}'\rangle - c|\mathrm{N}\rangle\big), \quad c = \langle \mathrm{N}|\mathrm{R}'\rangle. \tag{8}$$

A better procedure results from a diagonalization of the Hamiltonian in the subspace spanned by $|\mathrm{R}'\rangle$ and $|\mathrm{N}\rangle$:

$$|\widetilde{\mathrm{R}}\rangle = c_R^R|\mathrm{R}'\rangle + c_N^R|\mathrm{N}\rangle, \qquad |\widetilde{\mathrm{N}}\rangle = c_R^N|\mathrm{R}'\rangle + c_N^N|\mathrm{N}\rangle. \tag{9}$$

A central point in our treatment of the Roper is the freedom of the chromodielectric profile, as well as of the chiral meson profiles, to adapt to a $(1s)^2(2s)^1$ configuration. Therefore, quarks in the Roper experience mean fields which are different from the mean boson fields felt by the quarks in the nucleon.

The self-consistently determined fields shown in Fig. 1 depend noticeably on the quark source configuration. The $\chi$-field is almost insensitive to the $\sigma$-meson mass while the strength of the chiral fields increase with decreasing $\sigma$-meson mass. In Fig. 2 we show the quark radial profiles calculated self-consistently and, for the 2s state, also the radial profile calculated with the fixed background fields determined in the self-consistent calculation of the nucleon ground state (hereafter we call this approximation "frozen fields" calculation and denote it by "ff" to distinguish it from the self-consistent calculation, denoted by "sc"). In Table 1 we give the nucleon energy, $E_N$, and the Roper–nucleon energy splitting for various approximations. The 1s–2s level splitting corresponds to the ff calculation (in this case the boson fields do not contribute to the difference), while $\Delta E_R$ refers to the self-consistent calculations. In the latter case, the level splitting itself is reduced by 35% with respect to ff, but the total Roper–nucleon splitting is

Table 1
For two sigma masses, listed are the nucleon energy using (7) ($E_N$) and (9) ($\widetilde{E}_N$), the nucleon–Roper energy difference for fixed background fields (2s–1s), for the state (8) ($\Delta E_R$), for (13) ($\Delta E_{R*}$), and for (9) ($\Delta\widetilde{E}_R$); $\varepsilon_1$ is the energy of the lowest vibrational mode and $c_2$ its strength. All energies are in MeV

| $m_\sigma$ | $E_N$ | 2s–1s | $\Delta E_R$ | $\varepsilon_1$ | $\Delta E_{R*}$ | $c_2$ | $\widetilde{E}_N$ | $\Delta\widetilde{E}_R$ |
|---|---|---|---|---|---|---|---|---|
| 1200 | 1269 | 446 | 354 | 1090 | 353 | 0.05 | 1256 | 380 |
| 700 | 1249 | 477 | 367 | 590 | 364 | 0.12 | 1235 | 396 |

actually higher due to the increase of the potential energy of the fields and to the orthogonalization (8).

The ansatz (7) for the Roper represents the breathing mode of the three valence quarks with the fields adapting to the change of the source. There is another possible type of excitation in which the quarks remain in the ground state while the $\chi$-field and/or the $\sigma$-field oscillate. Such oscillations can be simply described if the ground state is taken in the form of a (projected) coherent state. We expand the field operators of the scalar bosons around their expectation value in the ground state $|\mathrm{N}\rangle$ (7):

$$\hat{\sigma}(\boldsymbol{r}) = \sum_n \frac{1}{\sqrt{2\varepsilon_n}}\varphi_n(r)\frac{1}{\sqrt{4\pi}}\big[\tilde{a}_n + \tilde{a}_n^\dagger\big] + \sigma(r), \quad (10)$$

where the operators $\tilde{a}_n$ annihilate the ground state, i.e., $\tilde{a}_n|N\rangle = 0$. (We write here explicitly only the vibrations of the $\sigma$-meson; for the $\chi$-field the derivation is analogous.) From $\tilde{a}(k)|N\rangle = \sqrt{2\pi\omega_\sigma(k)}\,\eta(k)|N\rangle$ one can obtain a simple expression for the annihilation (creation) operator of the $n$th mode: [1]

$$\tilde{a}_n = \int \mathrm{d}k\,\tilde{\varphi}_n(k)\big(\tilde{a}(k) - \sqrt{2\pi\omega_\sigma(k)}\,\eta(k)\big), \quad (11)$$

where $\tilde{\varphi}_n(k)$ is the Fourier transform of the $n$th mode in (10).

The stability conditions for the ground state require that the $\varphi_n$ and $\varepsilon_n$ satisfy the Klein–Gordon equation:

$$\left(-\nabla^2 + m^2 + \frac{\mathrm{d}^2V(\sigma(r))}{\mathrm{d}\sigma(r)^2}\right)\varphi_n(r) = \varepsilon_n^2\varphi_n(r). \quad (12)$$

Here $V$ stands for the potential originating from the term $\mathcal{L}_{q-\mathrm{meson}}$ and the potential parts of $\mathcal{L}_\chi$ and $\mathcal{L}_{\sigma,\pi}$ in (1). For the self-consistently determined profiles of the ground state we find that the potential in (12) is *repulsive* for the $\chi$-field and *attractive* for the $\sigma$-field. This means that there are no glueball excitation in which the quarks would act as spectators: the $\chi$-field oscillates only together with the quark field. On the other hand, the effective $\sigma$-meson potential supports at least one bound state with the energy $\varepsilon_1$ of typically 100 MeV below the $\sigma$-meson mass [2] (see Table 1). The lowest excited state is obtained by populating the lowest mode of the vibrator with one boson.

We can now extend the ansatz (8) by introducing

$$\big|\mathrm{R}^*\big\rangle = c_1|\mathrm{R}\rangle + c_2\tilde{a}_\sigma^\dagger|N\rangle, \quad (13)$$

where $\tilde{a}_\sigma^\dagger$ is the creation operator for this lowest vibrational mode. The coefficients $c_i$ and the energy are determined by solving the (generalized) eigenvalue problems in the $2\times 2$ subspace. The solution with the lowest energy corresponds to the Roper while the orthogonal combinations could be attributed to the second excited state with nucleon quantum numbers, the N(1710), provided the $\sigma$-meson mass is sufficiently

[1] The most general expression would involve the Bogoljubov transformation; however, the corresponding ground state would not be a simple coherent state. If we want to keep the simple ansatz which allows us to perform calculations of matrix elements, the expression is the most general transformation that preserves the ground state. Performing the Bogoljubov transformation leads to RPA equations; the present approach is therefore a simplified treatment of RPA excitations.

[2] The appearance of an attractive potential is not only a feature of the CDM, it appears in other chiral models in which the chiral fields are not constrained to the chiral circle; e.g., in the recent calculation of the nucleon in the Nambu Jona-Lasinio model with non-local regulators [16] the chiral fields in the center of the soliton turn out to be quite far away from the chiral circle, producing a strong attractive potential for the $\sigma$-meson.

small. In such a case the latter state is described as predominantly the $\sigma$-meson vibrational mode rather than the second radial excitation of quarks.

The energy of the Roper resonance is reduced when the lowest vibrational mode is included in the ansatz; the reduction is small due to the small coupling between the state (8) and the lowest vibrational state with the energy $\varepsilon_1$ (see Table 1). The orthogonal combination is practically at energy $E_N + \varepsilon_1$. The orthogonalization procedure (9) lowers the ground-state energy and increases the nucleon–Roper energy splitting with respect to $\Delta E_R$.

We now turn to the presentation of the electromagnetic nucleon–Roper transition amplitudes. Using the state vectors (9) the nucleon–Roper resonant electromagnetic transition amplitudes are readily evaluated. One usually introduces the resonant transverse helicity amplitude defined in the rest frame of the resonance as

$$A_{1/2} = -\zeta \sqrt{\frac{2\pi\alpha}{k_W}} \int \mathrm{d}^3\boldsymbol{r} \left\langle \widetilde{\mathrm{R}}_{+1/2,M_T} \middle| \boldsymbol{J}_{\mathrm{em}}(\boldsymbol{r}) \cdot \boldsymbol{\epsilon}_{+1} \times \mathrm{e}^{\mathrm{i}\boldsymbol{k}\cdot\boldsymbol{r}} \middle| \widetilde{\mathrm{N}}_{-1/2,M_T} \right\rangle, \tag{14}$$

and a scalar helicity amplitude

$$S_{1/2} = \zeta \sqrt{\frac{2\pi\alpha}{k_W}} \int \mathrm{d}\boldsymbol{r} \left\langle \widetilde{\mathrm{R}}_{+1/2,M_T} \middle| J^0_{\mathrm{em}}(\boldsymbol{r}) \times \mathrm{e}^{\mathrm{i}\boldsymbol{k}\cdot\boldsymbol{r}} \middle| \widetilde{\mathrm{N}}_{+1/2,M_T} \right\rangle, \tag{15}$$

where $\alpha = \mathrm{e}^2/4\pi = 1/137$ is the fine-structure constant, the unit vector $\boldsymbol{\epsilon}_{+1}$ is the polarization vector of the electromagnetic field, $k_W$ is the photon momentum at the photon point, $k_W = (M_{\mathrm{R}}^2 - M_{\mathrm{N}}^2)/2M_{\mathrm{R}}$, and $\zeta$ is the sign of the $N\pi$ decay amplitude [17]: $\zeta = \mathrm{sgn}\{\langle R(\frac{1}{2}\frac{1}{2}) \to \pi_a + N_b(M = -\frac{1}{2})\rangle/(1a\,\frac{1}{2}b|\frac{1}{2}\frac{1}{2})\}$, where $a$ and $b$ are the third components of pion and nucleon isospin, respectively. This sign has to be explicitly calculated within the model. Performing the multipole decomposition of the (transverse) electromagnetic field, $\boldsymbol{A}_{+1} = \boldsymbol{\epsilon}_{+1}\mathrm{e}^{\mathrm{i}\boldsymbol{k}\cdot\boldsymbol{r}}$, and using the Wigner–Eckart theorem, Eq. (14) becomes

$$A_{1/2} = \zeta \sqrt{\frac{\pi\alpha}{k_W}} \int \mathrm{d}^3\boldsymbol{r}\, \frac{3j_1(kr)}{r} \left\langle \widetilde{\mathrm{R}}_{1/2,M_T} \middle| \times \left[\boldsymbol{r} \times \boldsymbol{J}_{\mathrm{em}}(\boldsymbol{r})\right]_0 \middle| \widetilde{\mathrm{N}}_{1/2,M_T} \right\rangle. \tag{16}$$

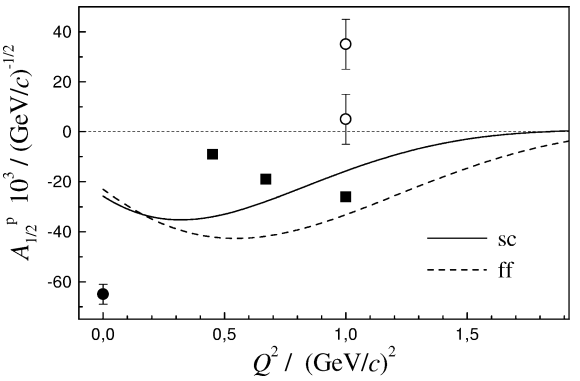


Fig. 3. Nucleon–Roper transverse helicity amplitude for charged states. The experimental point at $Q^2 = 0$ is the estimate of the PDG [18]. The solid squares result from the analysis of electroproduction data performed in [19]. The open circles also result from an analysis of electroproduction data [20]. The curves refer to self-consistent (sc) and frozen fields (ff) calculations. Parameter set as in Fig. 1.

Similarly, Eq. (15) becomes

$$S_{1/2} = \zeta \sqrt{\frac{2\pi\alpha}{k_W}} \int \mathrm{d}^3\boldsymbol{r}\, j_0(kr) \times \left\langle \widetilde{\mathrm{R}}_{1/2,M_T} \middle| J^0_{\mathrm{em}}(\boldsymbol{r}) \middle| \widetilde{\mathrm{N}}_{1/2,M_T} \right\rangle. \tag{17}$$

The electromagnetic operator in the CDM, $J^\mu_{\mathrm{em}} \equiv (J^0_{\mathrm{em}}, \boldsymbol{J}_{\mathrm{em}})$, contains a quark part and a pion part and reads:

$$J^\mu_{\mathrm{em}} = \sum_{i=1}^{3} \bar{q}_i \gamma^{\mu,(i)} \left(\frac{1}{6} + \frac{1}{2}\tau_0^{(i)}\right) q_i + \left(\boldsymbol{\pi} \times \partial^\mu \boldsymbol{\pi}\right)_0, \tag{18}$$

where the index 0 refers to the isospin third component.

Our results for the transverse helicity amplitudes for the charged and neutral states are shown in Figs. 3 and 4 for the parameter set $g = 0.03$ GeV, $M = 1.4$ GeV and $m_\sigma = 0.85$ GeV (the amplitudes for $m_\sigma = 0.7$ GeV and $m_\sigma = 1.2$ GeV are quantitatively similar to those shown in Figs. 3 and 4). Shown are the model predictions for the self-consistent calculations (using states (9)) and for ground state frozen fields (using states (7)). The experimental values at the photon point are the PDG most recent estimate [18] $A^p_{1/2} = -0.065 \pm 0.004\ (\mathrm{GeV}/c)^{-1/2}$ and $-0.040 \pm 0.010\ (\mathrm{GeV}/c)^{-1/2}$ for $A^n_{1/2}$. The pion contribution to the charged states only accounts for a few percent

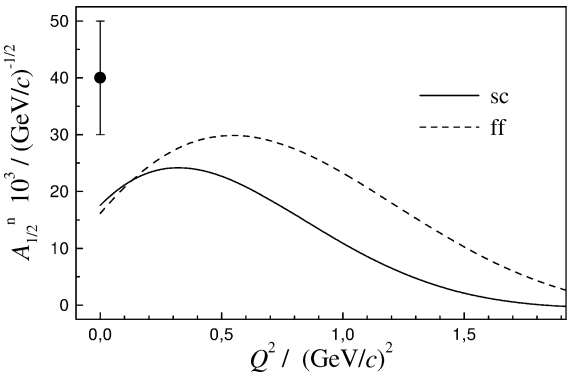


Fig. 4. Nucleon–Roper transverse helicity amplitude for neutral states. See also caption of Fig. 3.

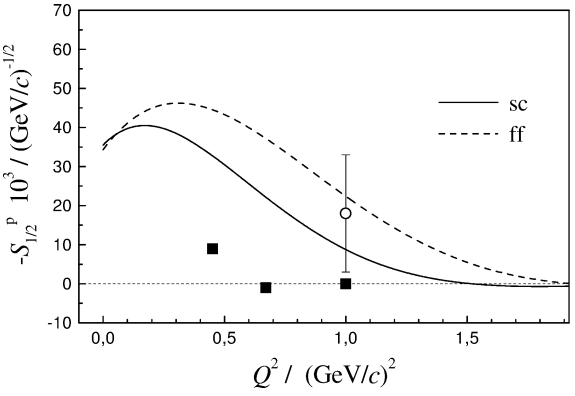


Fig. 5. Nucleon–Roper scalar helicity amplitude for charged states. See also caption of Fig. 3.

of the total amplitude. The large discrepancy at the photon point can be attributed to a too weak pion field in the model which we already noticed in the calculation of nucleon magnetic moments [14] and of the electroproduction of the $\Delta$ [10]. Other chiral models [9] predict a much stronger pion contribution which enhances the value of the amplitudes at the photon point. If we calculate perturbatively the leading pion contribution we also find a strong enhancement at the photon point; however, when we properly orthogonalize the state with respect to the nucleon, this contribution almost disappears.

In Fig. 5 we present the scalar helicity amplitudes for the proton; the amplitude for the neutron is very close to 0 and is not shown. No data are available which prevents any judgment of the quality of the approaches.

In CQM calculations [1,3,4] which incorporate a consistent relativistic treatment of quark dynamics, the amplitudes change the sign around $Q^2 \sim 0.2$–$0.5\ (\mathrm{GeV}/c)^2$. The amplitudes with this opposite sign remain large at relatively high $Q^2$, though, as shown in [3,4], the behavior at high $Q^2$ can be substantially reduced if either corrections beyond the simple Gaussian-like ansatz or pionic degrees of freedom are included in the model. Other models, in particular those including exotic (gluon) states, do not predict this type of behavior [5]. The present experimental situation is unclear. If in the future a more accurate experimental analysis confirms the change of the sign at low $Q^2$, this would certainly be a success of the CQM; if, however, this is not the case, one should not rule out conventional quark model explanations in favor of the exotic states as proven by our calculation. Our model, similarly as other chiral models [8,9], predicts the correct sign at the photon point, while it does not predict the change of the sign at low $Q^2$. Let us also note that with the inclusion of a phenomenological three-quark interaction Cano et al. [4] shift the change of the sign to $Q \sim 1\ (\mathrm{GeV}/c)^2$ beyond which, in our opinion, predictions of low energy models become questionable anyway.

It is interesting to note that, in the self-consistent calculation, there is a substantial contribution to the amplitudes from the admixtures of $|\mathrm{N}\rangle$ in $|\widetilde{\mathrm{R}}\rangle$ and of $|\mathrm{R}'\rangle$ in $|\widetilde{\mathrm{N}}\rangle$ (see expressions (9)). Such contributions are not present in the calculation with frozen profiles (since the states (7) are already orthogonal) but nonetheless, both approaches yield similar results for the amplitudes, indicating that the results are not very sensitive to small variations of the profiles. We should stress that we have made no attempt to fit the electroexcitation amplitudes nor the excitation energy of the Roper resonance but have used model parameters that were fixed in the ground state calculation.

We do not give the amplitudes for the second excited state N(1710). As we have already mentioned, provided that the $\sigma$-meson mass is sufficiently small, this state can be dominated by a component carrying one quantum of $\sigma$-meson vibration. Such a picture predicts very small production amplitudes since mostly the scalar fields are excited. The presence of $\sigma$-meson vibrations is consistent with the recent phase

shift analysis by Krehl et al. [7] who found that the resonant behavior in the $P_{11}$ channel can be explained solely through the coupling to the $\sigma$–N channel, without assuming any internal (i.e., quark) radial excitation of the nucleon. In our view, radial excitations of quarks are needed in order to explain relatively large electroproduction amplitudes, which would indicate that the $\sigma$–N channel couples to all nucleon $(1/2)^+$ excitations rather than be concentrated in the Roper resonance alone.

To conclude, though our model gives only a qualitative picture of the lowest nucleon radially excited states and their electroproduction amplitudes, it yields some interesting features, in particular the possibility of $\sigma$-meson vibrations, not present in other calculations. Its main advantage over other approaches is that all properties, including the EM amplitudes and the resonance decay, can be calculated from a single Lagrangian without introducing additional assumptions; it also allows us to exactly treat the orthogonalization of states which is particularly important in the description of nucleon radial excitations. It would be instructive to check our predictions in other chiral models and extend the present calculation to include other radially excited states such as radial excitations of the $\Delta$.

## Acknowledgements

This work was supported by FCT (POCTI/FEDER), Lisbon, and by The Ministry of Science and Education of Slovenia. We thank S. Širca and M. Rosina for useful discussions.

## References

[1] S. Capstick, Phys. Rev. D 46 (1992) 2864;
S. Capstick, B.D. Keister, Phys. Rev. D 51 (1995) 3598.
[2] H.J. Weber, Phys. Rev. C 41 (1990) 2783.
[3] F. Cardarelli, E. Pace, G. Salmè, S. Simula, Phys. Lett. B 397 (1997) 13.
[4] F. Cano, P. González, Phys. Lett. B 431 (1998) 270.
[5] Z. Li, V. Burkert, Z. Li, Phys. Rev. D 46 (1992) 70;
E. Carlson, N.C. Mukhopadhyay, Phys. Rev. Lett. 67 (1991) 3745.
[6] W. Broniowski, T.D. Cohen, M.K. Banerjee, Phys. Lett. B 187 (1987) 229.
[7] O. Krehl, C. Hanhart, S. Krewald, J. Speth, Phys. Rev. C 62 (2000) 025207.
[8] Y.B. Dong, K. Shimizu, A. Faessler, A.J. Buchmann, Phys. Rev. C 60 (1999) 035203.
[9] K. Bermuth, D. Drechsel, L. Tiator, Phys. Rev. D 37 (1988) 89.
[10] M. Fiolhais, B. Golli, S. Širca, Phys. Lett. B 373 (1996) 229;
L. Amoreira, P. Alberto, M. Fiolhais, Phys. Rev. C 62 (2000) 045202.
[11] P.A.M. Guichon, Phys. Lett. B 163 (1985) 221;
P.A.M. Guichon, Phys. Lett. B 164 (1985) 361.
[12] M.C. Birse, Prog. Part. Nucl. Phys. 25 (1990) 1;
T. Neuber, M. Fiolhais, K. Goeke, J.N. Urbano, Nucl. Phys. A 560 (1993) 909.
[13] A. Drago, M. Fiolhais, U. Tambini, Nucl. Phys. A 588 (1995) 801.
[14] A. Drago, M. Fiolhais, U. Tambini, Nucl. Phys. A 609 (1996) 488.
[15] B. Golli, M. Rosina, Phys. Lett. B 165 (1985) 347;
M.C. Birse, Phys. Rev. D 33 (1986) 1934.
[16] B. Golli, W. Broniowski, G. Ripka, Phys. Lett. B 437 (1998) 24.
[17] J. Babcock, J.L. Rosner, Ann. Phys. (N.Y.) 96 (1976) 191.
[18] D.E. Groom et al., Particle Data Group, Eur. Phys. J. C 15 (2000) 1.
[19] C. Gerhardt, Z. Phys. C 4 (1980) 311.
[20] B. Boden, G. Krosen, in: V. Burkert et al. (Eds.), Proceedings of the Conference on Research Program at CEBAF II, CEBAF, USA, 1986.